A Computationally Efficient Computer-Aided Design Strategy for Iterative Combat Helmet Design and Analysis

Robert Saunders[1]
U.S. Naval Research Laboratory,
4555 Overlook Avenue SW,
Washington, DC 20375
e-mail: robert.saunders@nrl.navy.mil

Alex Moser
U.S. Naval Research Laboratory,
4555 Overlook Avenue SW,
Washington, DC 20375
e-mail: alex.moser@narl.navy.mil

Peter Matic
U.S. Naval Research Laboratory,
4555 Overlook Avenue SW,
Washington, DC 20375
e-mail: peter.matic@nrl.navy.mil

Assessing combat helmet ballistic performance is a costly endeavor using either an experimental or a computational process. Experimental assessment requires many iterations and helmets to acquire a sufficient data set. To circumvent this, computational simulation is incorporated into the design process to supplement a few experiments. However, due to the complex constitutive response of the helmet (anisotropic elasticity, plasticity, damage initiation and evolution, and failure), it is computationally costly to run many ballistic impact simulations. The goal of this work is to develop a computer-aided design (CAD) software to rapidly analyze combat helmets undergoing a ballistic impact. The software considers a representative mix of potential threats, helmet geometry modifications and additions, brain functional anatomy, and injury considerations. The resulting software demonstrates that a given helmet can be analyzed in a matter of minutes on a standard desktop computer and parametric studies can be completed in a matter of hours. The results of the CAD software show how helmet design parameters such as helmet shell materials, geometry, and ceramic appliques all affect helmet ballistic performance.
[DOI: 10.1115/1.4041975]

Keywords: ballistic, efficient, iterative, combat helmet

Introduction

The cost of designing, fabricating, and physically testing a prototype combat helmet to assess performance against ballistic threats is high. Methods for detailed helmet ballistic impact computational simulations to understand the relative operational benefits and costs in terms of injury performance are advancing but require high performance computing and long run times [1–9]. A broad range of test data and models of varying complexity and precision are generally used to select helmet materials and define geometric configuration for complex threat environments of interest [10–12]. These methods do not generally meet the needs of iterative design processes to rapidly evaluate candidate helmet configurations.

The objective of this work is to develop a computer-aided design (CAD) software application to rapidly evaluate helmet geometry and material performance in the context of overall ballistic impact protection. This software is applied to evaluate helmet protection options against a representative mix of ballistic threats and a mix of helmet geometries. Performance will be formulated and presented in terms of possible head injuries from nonpenetrating helmet impacts. A particular goal is to assess helmet coverage of the brain volume in terms of its functional anatomy regions and to incorporate three-dimensional brain data into the CAD software application.

To meet these objectives, the program incorporated brain functional anatomy descriptions, experimental data on material ballistic performance; first-order models of the impact events and head–helmet dynamic response; and medical data on head motion, injury type, and severity. The approach uses a set of 104 points in the brain and spinal column and an omni-directional set of 3000 ballistic projectile origination points. The combined resolution of these two point sets is useful and sufficient to assess the effects of small changes in the relatively constrained helmet geometry parameter trade space. Helmet back face deflection (BFD) and head injury criterion (HIC) from head–helmet dynamics were each used to estimate the abbreviated injury scores (AIS) for a standard set of head injuries.

These methods are integrated into a CAD package that is modular, quick to execute, and able to provide insights for helmet design. The assumptions and simplifications made in this effort ensured that the MATLAB-based package is computationally efficient for short run times on a personal computer. It is recognized that more comprehensive data and descriptive models will be valuable to the effort and can be incorporated as needed. This approach generates fast analysis and performance comparisons among the proposed helmet designs. A single design can be analyzed in minutes, and a parametric study completed in hours.

Combat Helmet Analysis Architecture

The helmet CAD software application was developed using MATLAB to be a modular program for quick combat helmet design analysis. A set of specialized software modules (Fig. 1) describes the head and helmet geometry and physical properties, the ballistic threat environment, the ballistic impact back face deflection and dynamic response of the head–helmet system, and the predicted injury due to the ballistic impact. These elements integrated into the CAD software application support definition of the helmet design trade-space and associated optimization strategies.

Head–Helmet System. First among the helmet CAD modules, we have the head and helmet descriptions. The geometry of both the head and the helmet can be obtained in a number of ways but only requires the final format input to be a digital stereolithography (STL) file. The STL files can be obtained from a number of
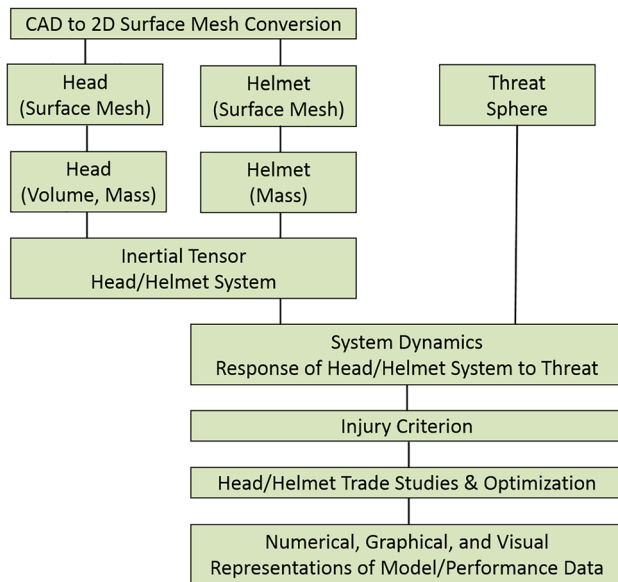
Fig. 1 Helmet CAD analysis architecture and flow chart

solid modeling software programs or can be generated from 3D images.

Anthropomorphic Head. The head and neck surface and volume models were developed from an existing head, neck, and torso surface rendering. The surface rendering conformed to nominal anthropomorphic dimensions recently documented for the United States Marine Corps population [13]. In addition to a geometric surface definition, the head is given a volume generated on a Cartesian voxel grid. A first-order adaptive meshing algorithm was used to generate voxels that approximately matched the surface mesh. The throat and nasal cavities were assumed to be of negligible volume in this model. Using the average mass density of a human head and the voxels generated, a mass of 6.1 kg was obtained along with the center of mass and inertia tensor needed for the analysis. The geometry of the head and neck is shown in Fig. 2.

A set of points representing geometric regions of the brain was compiled for placement in the model. It is essential that this set of brain points has sufficient resolution capable of supporting helmet design parametric analyses while not being so large a set as to generate undesirable computer run times. A set of between 50 and 150 points representing the brain volume was estimated to be sufficient to meet this objective. This range was chosen based on the time required to run a complete analysis of the software.
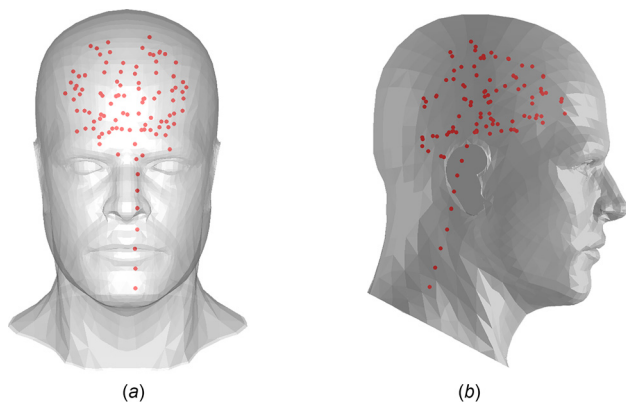
A set of 104 total representative brain points was used to define the head's nervous system. The set of brain points was generated using the Brodmann formalism describing brain functional anatomy by region of the cerebrum, supplemented by additional recent literature on cerebellum function, and by information on the upper spinal cord coordinates. In the cerebrum, 78 distinct Brodmann regions, 39 in each hemisphere, were implemented using centroid values for each region as discussed in the literature [14–16]. An additional 17 points in the cerebellum and nine points in the brain stem and spinal cord completed the set of 104 points. The points chosen, based on Brodmann points, are convenient since the number of points lies within the 50–150 point range identified previously. However, the brain could be described by any number of points the analyst chose to use. For instance, the 189 points identified by Oishi et al. [17] could have been used if a longer analysis time was deemed acceptable.

Combat Helmet Description. Five representative combat helmets are utilized in this work to compare helmet geometry effects on helmet performance. STL files of each helmet were obtained using a NextEngine Desktop 3D (Model 2020i) scanner. Solid white dots were placed on the helmet exterior surface as reference points to aid registration of overlapping scan segments. The scan segments were stitched together and scan mesh resolution reduced to a density of approximately 500 elements per helmet, appropriate to capture the local helmet curvatures needed for the impact obliquity calculations.

The measured helmet mass and surface area were used to determine an areal density for each helmet element in the analysis. The mass distribution over the helmet was used to calculate the helmet center of mass and inertia tensor used for the analysis. Additionally, modifications to these helmets, for parametric analysis of geometric design features, were made using the MESHLAB application to manipulate STL files.

The crown area of the head and neck surface model was used with each helmet model to establish head-to-helmet spacing in the analysis. Physically, the helmet suspension determines this spacing and the standard pad suspension was used in this work. (The pads themselves are not explicitly modeled in this work.) An example of the helmet elements used to establish spacing is identified in Fig. 3. This region of the helmet represents the area where padding would normally be seated and in contact with the head. The positioning was determined by an iterative process achieving a standard mean head-to-helmet spacing of 19 mm (0.75 in) and minimizing the spacing standard deviation. The spacing used is representative of the stand-off distance associated with common pad suspension systems. The positioning process involved translation, rotation, and minor helmet dimensional scaling to achieve the spacing mean and standard deviation objective.

Fig. 2 Anthropomorphic head with brain functional regions represented by 104 brain and spine point set: (*a*) front view and (*b*) side view
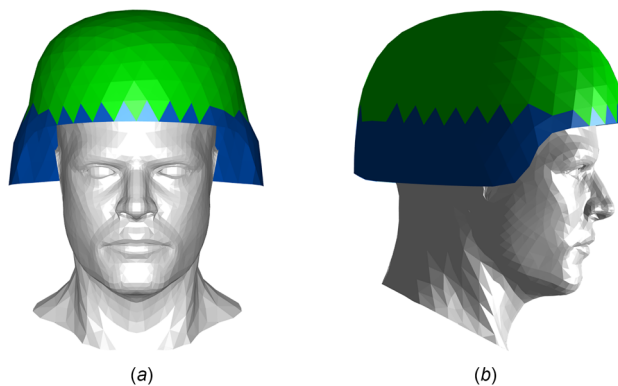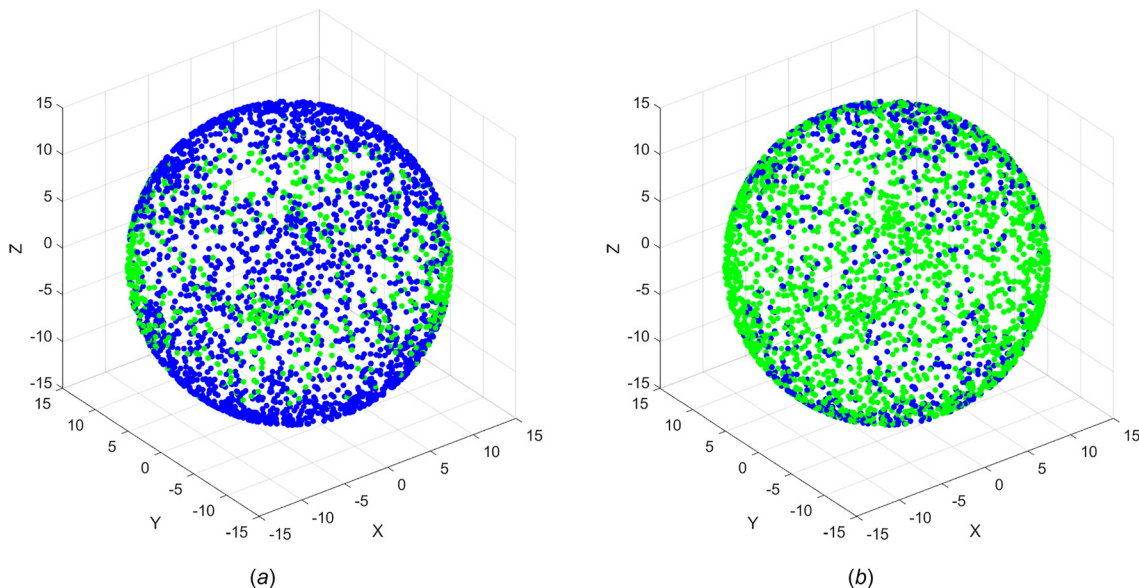

Fig. 3 Anthropomorphic head with representative combat helmet positioned. The green (light) color indicates elements that were used to position the helmet on the head: (*a*) front view and (*b*) side view.

Fig. 4 Ballistic projectile threat sphere showing Gaussian distribution of fragment (blue/dark): small arms (green/light) ratios: (a) 75:25 and (b) 25:75

Table 1 Summary of possible combinations of head, helmet, and threat combinations with the possible response

Impacts	9 mm	7.62 mm
Direct head	Catastrophic injury	Catastrophic injury
Aramid helmet region	Partial penetration/possible injury	Complete penetration/catastrophic injury
Aramid plus applique helmet region	Partial penetration/possible injury	Partial penetration/ possible injury

An aramid helmet shell was used as the baseline geometry and ballistic protection level in this work and is referred to as "helmet A." Its performance is compared to the performance of (i) four commercially available helmet designs (referred to as helmets B–E), (ii) six parametric modifications to the baseline helmet A geometry, and (iii) ceramic applique added to helmet A by zones on the shell. The ceramic applique is based on a commercial product (manufactured by Velocity Systems, Dulles, VA) and is designed to improve helmet performance against more substantial threats at the expense of increased helmet mass.

Threat Sphere. The threat sphere consists of 3000 ballistic projectile origination points. Each of these points is randomly disturbed over a sphere with 15 m radius. This distance was chosen to minimize trajectory parallax effects. The threat sphere is centered on the head and each point on the sphere is paired with each brain point, yielding 312,000 possible trajectories. Each point on the sphere is assigned a projectile mass and speed. In this work, we consider both isotropic and nonisotropic threat spheres consisting of one or multiple threats, respectively. Specific threats are 8.04 g 9×19 mm^2 full metal jacket and a 7.97 g 7.62×39 mm^2 mild steel core small arms projectile. The 9 mm threat is referred to as the "fragment" or "9 mm" threat, while the 7.62 mm threat is referred to as the "small arms" or "7.62 mm" threat in this discussion. The 9 mm threat is given an impact speed of 364 m/s, while the 7.62 mm threat is given an impact speed of 739 m/s. The term fragment is used interchangeably with 9 mm in this work, because it is assumed that the 9 mm threat has approximately the same mass and velocity of a fragment from an explosive device detonation.

An isotropic threat sphere is defined as either entirely the 9 mm fragment or the 7.62 mm small arms threat. The nonisotropic threat spheres consist of both threat types in different ratios. The ratios of 9–7.62 mm are expressed as x: $(100x)$, where x ranges from 0 to 100. Therefore, a threat ratio of 100:0 is 100% fragments and a ratio of 0:100 is 100% small arms. Intermediate

values, such as 50:50, were expressed on the sphere using a Gaussian probability distribution, so small arms threats had a higher likelihood of occurring at points on the threat sphere associated with the ground horizon, i.e., along the transverse plane of the head. Two examples of nonisotropic threat distributions can be seen in Fig. 4. The probability distribution serves the purpose of representing a notional tactical situation with adversary fragment threats dominant from artillery airburst fragments coming from the top, buried explosive device fragments coming from the bottom, and adversaries with small arms operating on the ground along the horizon.

Head–Helmet Threat Response. The interaction between the threat and the head–helmet system is determined only when the trajectories defined by a threat point/Brodmann point pair intersect the combat helmet. The helmet impact performance is quantified by the materials ballistic resistance velocity (V_0) and the BFD [18]. Both quantities are commonly measured based on test data obtained at 0 deg obliquity (normal to the helmet). To account for non-normal impacts, the 0 deg BFD is assumed to be scaled by the cosine of the obliquity [19]. A 90 deg obliquity indicates a tangential glancing impact and generates zero BFD. In this work, the helmet polymer shell overmatches the fragment projectile, while the helmet polymer shell plus applique overestimates both fragments and small arms projectiles.

In the general case of mixed fragment and small arms threats and helmets with polymer shell and ceramic applique, six different types of impact events can be generated. These cases are summarized in Table 1. In the first two cases, we simply have the 9 mm or 7.62 mm threat impact on the head directly, so the threat does not strike the helmet. The events are considered catastrophic and excluded from further analysis.

In the next case, the 9 mm threat strikes the helmet in a region without applique over the baseline aramid. This threat is considered to be matched to the helmet so $V_{\text{threat}} \leq V_0$ and no complete
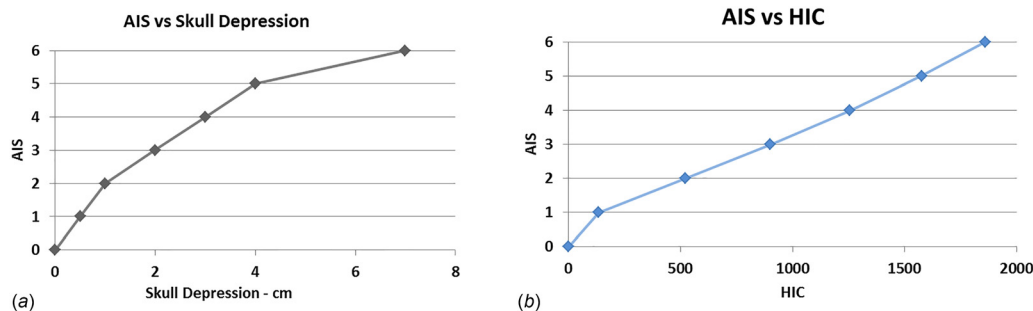
Fig. 5 Relationships of (*a*) dynamic skull depression (leading to skull fracture onset) to BFD-AIS [20,22] and (*b*) head injury criteria to Accel-AIS for focal and diffuse [22] brain injuries

penetrations of the helmet occur. The 9 mm threat produces a helmet BFD of 25.4 mm from a normal impact. If the 7.62 mm round strikes in the baseline helmet region, the round is considered to be over-matched to the helmet so $V_{threat} > V_0$ and a complete penetration of the helmet occurs producing a catastrophic event. When the 7.62 mm round strikes the helmet with an applique applied, the round is evenly matched to the helmet. The 7.62 mm impact against the applique produces a BFD of 16.5 mm. In the final case, the 9 mm strikes the applique and is undermatched. No BFD data were available for this instance but it is assumed, conservatively, that this case produces partial penetration with a 16.5 mm BFD.

For partial penetrations, two separate events can contribute to a possible injury: (i) the dynamic head-to-helmet spacing which defines whether the helmet shell BFD will make contact with the head and (ii) the acceleration of the head–helmet system as the threat decelerates. The dynamic BFD is the distance obtained by considering the static helmet spacing minus the BFD attenuated by the threat obliquity. If this value is negative i.e., the BFD from the impact is greater than the static helmet distance to the head, then it is assumed that the helmet contacts with the skull. Depression and fracture of the skull may occur. This is a simplified analysis that does not account for any biological components, except the skull, or any corresponding constitutive responses. It does give insight into the performance of a helmet and the importance of placement and spacing on the warfighter's head.

The deceleration of the projectile and the acceleration of the head–helmet system to a final post impact velocity (and zero residual acceleration) for the projectile–head–helmet system is determined using conservation of linear momentum. The acceleration-time profile of each projectile type impacting the helmet is assumed to occur over a known time interval characteristic of the ballistic threat and helmet material system. The acceleration-time profile is also assumed to be in the form of a truncated Gaussian profile in this time interval, describing the increasing and decreasing deceleration of the projectile from initial strike to final velocity. The use of such a standard analytical form for the impact event ensures rapid computation. Angular accelerations and angular momenta are not included in this discussion but are included in the analysis and may be used in the future to consider rotational acceleration contributions to brain injury.

The extent of helmet coverage prevents many direct head impacts for low energy threats such as the 9 mm round, but these impacts to the helmet can still generate a range of injuries due to either the dynamic BFD or the head acceleration. The quantification of these injuries is accomplished through a survey of current literature. The nature of this literature, on both military and civilian injuries, requires careful consideration of how biomechanical engineering parameters and data can best be used with medical parameters and data. This includes the quantity and quality of injury data, the degree to which a mechanistic understanding of the injury exists, and medical diagnostic methods and parameters. A survey of studies was useful and relevant in general qualitative terms to understand frequency and incidence of trauma. Most studies with statistically relevant data are surveys of large civilian

injury data records associated with a variety of blunt impacts. While not military data, the form of the data was useful and relevant in general terms to develop the methods here and use additional data in the future. Individual head trauma studies generally focus on only a subset of head injuries. However, the linkages between the biomechanical and medical aspects are in many cases complicated and incomplete at this time.

For these reasons precisely, the injury criteria developed from the diagnostic metrics were used rather than clinical data. A reasonably unified, consistent, and practical set of ten injuries with associated injury criteria was developed by integrating the results of civilian trauma studies in the literature. The selected criteria were based on skull fracture type diagnosis, dimensional diagnostic metrics associated with clinically imaged blood volumes for internal focal head injuries, and loss of consciousness (LOC) clinical diagnostic metrics associated with internal diffuse head injuries [20–22]. The studies used for this effort collectively covered the full set of head injuries of concern, were comprehensive enough to provide statistically relevant data and insight for the injuries being studied, and provided this data in a form to support the linkage of BFD and HIC to AIS diagnostic metrics.

Skull fractures can be generated by helmet back face deflection contact with the head and deformation of the skull. Injury severity for this analysis is based on the magnitude of the skull depression. The typical thickness of the skull is approximately 7 mm. A relatively small amount of skull depression, less than 5 mm, is assumed not to initiate a skull fracture. Skull depression beyond 5, 10, and 20 mm is assumed to initiate progressively linear (elastic fracture with no residual displacement), depressed (patterned or contained fracture with displacement), and compound (dispersed fracture with displacement) fracture type classifications with increasing AIS severity, respectively (Fig. 5(*a*)). A "BFD-AIS" value for each helmet is defined from the minimum dynamic head-to-helmet spacing values, i.e., maximum skull depression, from all impacts on each helmet. While not a "cause and effect" mechanism, it associates maximum skull depression with injury severity. That value is extended to the full set of head injuries as a conservative metric for BFD contact effects.

The HIC value calculated from the head–helmet acceleration following impact for each helmet was used to define an "Accel-AIS" value (Fig. 5(*b*)). The BFD-AIS and the Accel-AIS were used to independently calculate diagnostic dimensional and LOC metrics for focal and diffuse head injuries. Using AIS to predict injury does not signify each of the nine injuries will occur, only that it is possible for one or more to occur.

Six focal injuries are associated with arterial or venous blood vessel damage and associated pooling of blood. Those from epidural, subdural, and subarachnoid hematomas may occur in the vicinity of the impact. Deeper in the brain, blood vessel damage is associated with intraventricular and intraparenchymal hematomas that may occur. Contusions may generate blood pooling and tissue damage. Some associated coup countercoup events may also generate injury away from the area of impact. These injuries can be imaged by radiological means and quantified by their length, area,
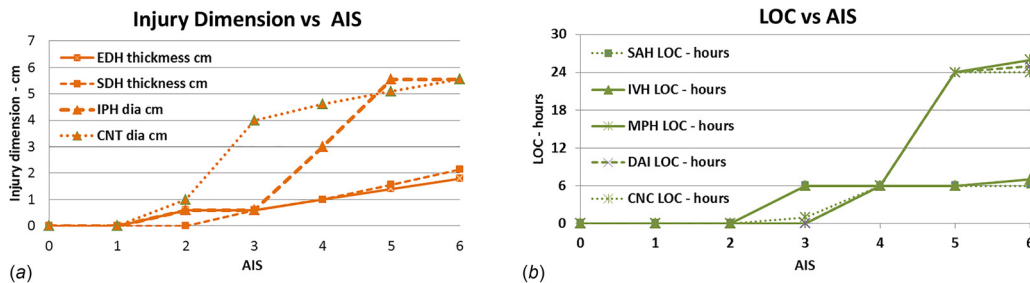
Fig. 6 Abbreviated injury scores to produce (*a*) characteristic injury dimension and (*b*) LOC intervals for focal and diffuse injuries [21]
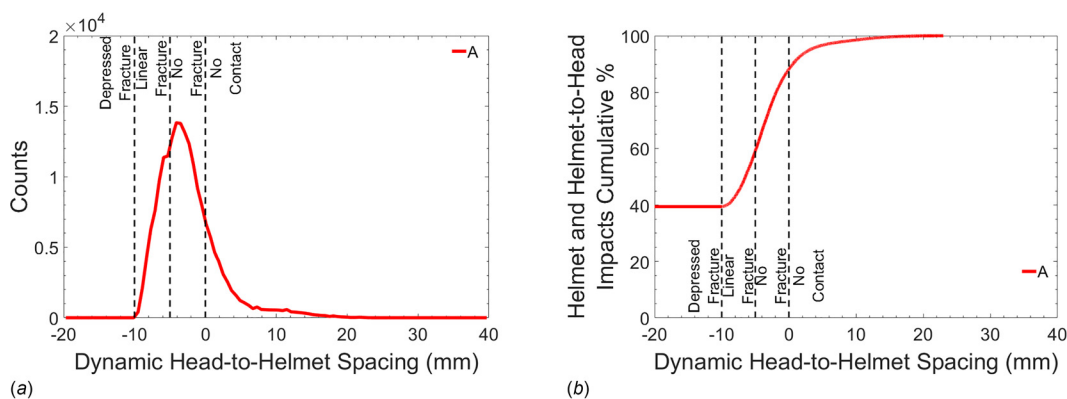

Fig. 7 Baseline helmet A performance for dynamic head-to-helmet spacing: (*a*) helmet-to-head impact histograms and (*b*) all impact cumulative percentages (initial percentages are direct head impacts) for strike from 9 mm strike velocity of 364 m/s

and volume. The length metrics for these injuries were the most consistent across standard diagnostic criteria for the injuries and used here with AIS (Fig. 6(*a*)) [21].

Three diffuse head injuries are associated with multiple petechial hemorrhages, diffuse axonal injury, or concussions. Radiological diagnosis is often difficult or impossible to obtain so LOC is a common correlative indicator under a set of diagnostic criteria for each injury and is also used here with AIS (Fig. 6(*b*)).

Results and Discussion

As is common in analyses where large datasets are generated, the value of the data to the user is governed by the way in which the data are extracted, displayed, interpreted, and used to guide the design process. The modular nature of this program allows intermediate results to be obtained before proceeding to the next module. Data reported in this paper only summarize a subset of the tabulated data and graphs generated. For further results and discussion, the interested reader is referred to Refs. [23] and [24].

To begin, we focus on only the baseline helmet, helmet A, against a 9 mm isotropic threat sphere given a nominal velocity of 364 m/s, based on V_0 of the helmet. The 7.62 threat is not considered without an applique as 100% of the shots penetrate the helmet and directly impact the head. The computational analysis time for this simple case of a single helmet against a single threat sphere distribution took approximately 90 s to complete. This is characteristic of each analysis and will scale linearly with the number of helmets analyzed, the number of threat sphere distributions analyzed, and the number of triangular elements used to mesh the helmet.

From this analysis, we examine the histogram and cumulative histogram of dynamic head-to-helmet spacing (Fig. 7) for helmet A. Figure 7(*a*) shows the thresholds of 5, 10, and 20 mm to estimate skull fracture onset (i.e., linear, depressed, and compound); we can see some linear fracture and no depressed fractures are

predicted to occur from any combination and the largest number of points lie in the −5 to 0 mm range where contact is predicted but no injury. This is indicative of an overall good performing helmet, where an ideal BFD performance would have no contact as characterized by no data points below 0 mm dynamic spacing. From Fig. 7(*b*), the position of the cumulative histogram to the right is indicative of higher dynamic spacing value. Furthermore, from this representation, we show the percentage of impacts that do not contact the helmet and also the percentage that are direct impacts to the head, and therefore, catastrophic (represented by the vertical offset on the left side of the graph).

The BFD-AIS and Accel-AIS predictions for the nine internal head injuries are shown in Fig. 8 for helmet A. The minimum dynamic head-to-helmet spacing value for the helmet, in this case approximately −9.5 mm, generates BFD-AIS values. The HIC value of the helmet, in this case 254, generates Accel-AIS values. Comparing the two sets of predictions shows that both sets of injury levels are of relatively low severity below an AIS value of 2. The predicted AIS values and associated injury diagnostic dimensions and loss of consciousness times are useful comparators of helmet performance and for helmet design.

With the results for baseline helmet A established, three comparative studies of other helmet materials, geometries, and additions are performed and their results plotted and compared.

Study 1—Commercially Available Helmet Comparison. In the first study, the baseline helmet A is compared to four other commercially available helmets of different geometries and materials as shown in Table 2. Each of the helmets is made of either the ballistic material aramid or ultrahigh molecular weight polyethylene (UHMWPE). The specific material and manufacturer differences mean that each helmet has a dissimilar BFD and V_0 combination. The 9 mm threat was originally given a nominal velocity of 364 m/s, based on V_0 of the baseline helmet A. To
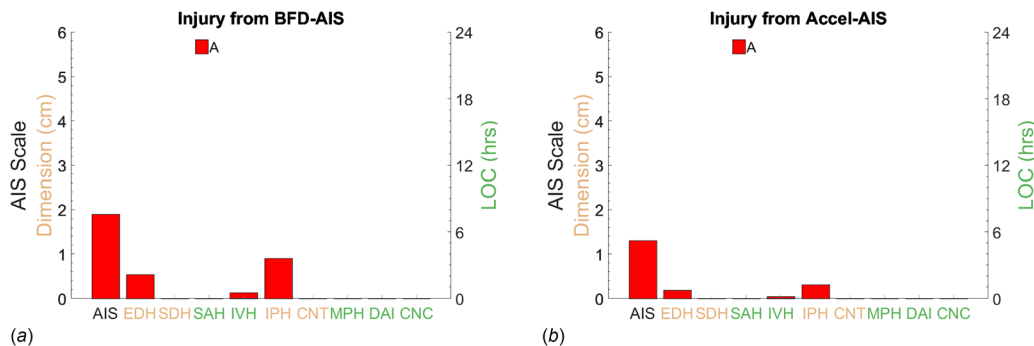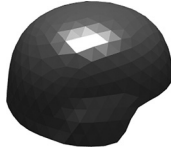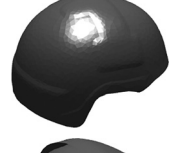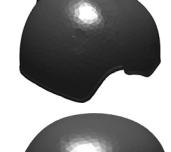
Fig. 8 Baseline helmet A performance of (*a*) BFD-AIS and (*b*) Accel-AIS and associated head injuries diagnosed by dimension or LOC duration for strike from 9 mm strike velocity of 364 m/s

Table 2 Helmet A compared to four other commercially available helmets

Helmet	Material	Area (cm^2)	Mass (kg)	V_0 (m/s)	Geometry
A (baseline)	Aramid	1077.3	1.16	364	
B	UHMWPE	1093.7	1.18	427	
C	UHMWPE	1043.6	0.92	366	
D	UHMWPE	1281.6	0.86	364	
E	Aramid	1000.7	0.94	344	

Note: V_0 given corresponding to a normal impact that produces a BFD of 25.4 mm.

directly compare the helmets, the 9 mm threat impact velocity used is 344 m/s, taken from the lowest V_0 of any helmet in the full group of helmets. The BFDs are scaled based on kinetic energy of the impact using the lowest V_0. For example, in the case of baseline helmet A, the original BFD generated was 25.4 mm from the 364 m/s V_0. The new BFD is 22.4 mm for the 9 mm threat with the lower 344 m/s velocity.

The same analysis described previously is performed on each helmet. The results are shown in Fig. 9. Helmets A and B with similar geometries and different materials have quite significant performance differences. Over 50% of the impacts on helmet A cause either contact or fracture where <5% of those on helmet B cause contact and no impacts cause fracture. Similar differences are seen between aramid helmets A (<5% cause linear fracture) and E (15% cause linear fracture) as well as UHMWPE helmets B (0% cause fracture), C (<5% cause fracture), and D (>30% cause fracture), which use similar materials with dissimilar geometries.

Figure 9(*b*) shows that helmets B and D perform the best relative to the minimum dynamic spacing and the number of catastrophic hits, respectively. Examining the injury metrics, there is little difference in the HIC-based injury of Fig. 9(*d*) but quite significant difference in the BFD-based injury of Fig. 9(*c*). In particular, contusions and intraparenchymal hematomas injuries are significant for helmet D and to a lesser extent helmet E. The HIC values for the five helmets range from 201 (helmet B) to 225 (helmet D). The AIS value based on BFD, while significantly different relative to one another, is still in the AIS range of approximately 1–2 and represents relatively minor injuries.

To further quantify the performance of each helmet against one another, the value and range of values of mean dynamic spacing are compared to the HIC as shown in Fig. 10. While helmet D had the fewest number of catastrophic impacts, it had the lowest mean dynamic spacing and highest HIC value. This is caused by the low mass, which is a result of tight fit over the head, less coverage
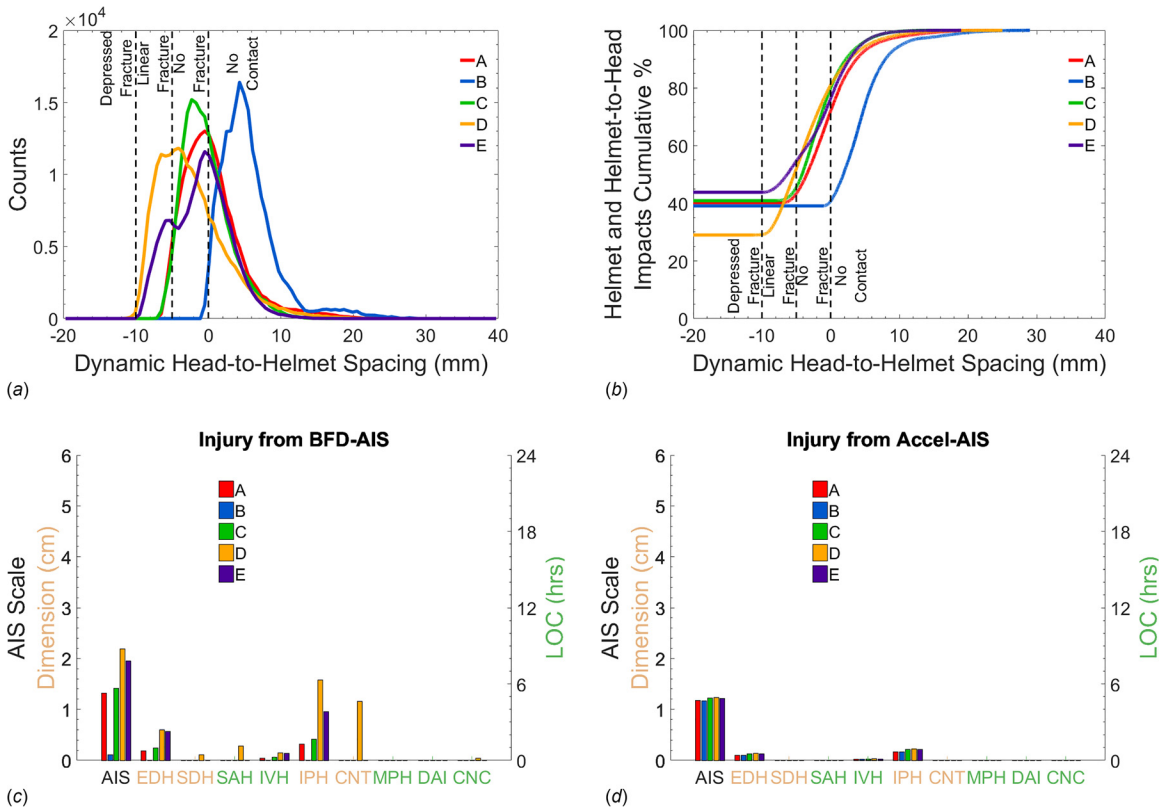
Fig. 9   Five helmet comparative performance for 9 mm strike velocity of 344 m/s: (*a*) helmet impact histograms, (*b*) all impact cumulative percentages (initial percentages are head impacts), (*c*) BFD-AIS, and (*d*) Accel-AIS and associated head injuries diagnosed by dimension or LOC duration

over the ears, and closer contouring of the nape region. (These effects are greater than the midline coverage of the helmet, which increases the area.) While a helmet that closely follows the contours of the head seems ideal, the tight fit leads to close static spacing all around, thus giving lower dynamic spacing. The helmet masses, as expected, correspond well with the predicted HIC value in which the highest mass had the highest performance. When designing helmets, a low HIC value is desired. However, the extra weight burden the Warfighter must bear should be considered. Thus, a lower mass is desirable and some tradeoff in injury risk may be acceptable.
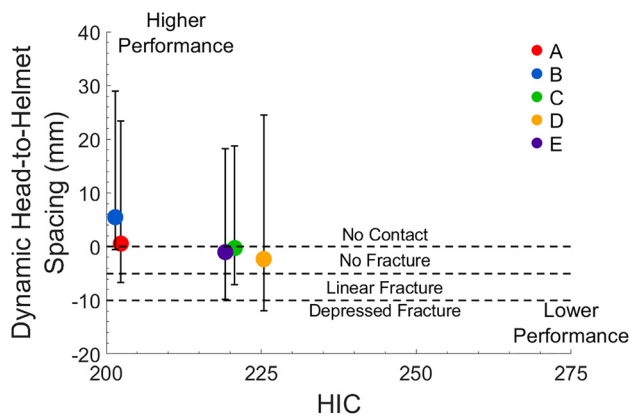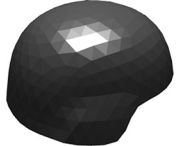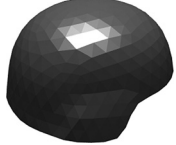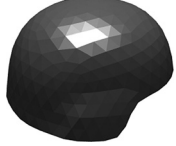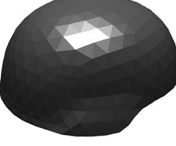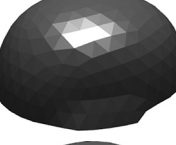

Fig. 10   Helmets A–E comparative analysis summary plot of dynamic spacing versus HIC value. Mean value and min–max represented by symbol and range for 9 mm strike velocity of 344 m/s.

Study 2—Parametric Helmet Geometry Modifications. In the second study, baseline helmet A is modified by independently changing the size of the ear opening, the nape extension, or the static helmet spacing. For naming each helmet configuration, the side opening over the ear is designated by an *S*, the nape extension an *N*, and the static helmet-to-head spacing an *H*. Each designation is followed by a two-digit number to indicate the size of the modification in millimeters. The baseline helmet A is given the designation A-S00-N37-H19 for a 0 mm side opening, a nape extending 37 mm below the brim and an average 19 mm static spacing. The designations for the others are summarized in Table 3, where two larger values for ear opening (to provide greater auditory situational awareness), two smaller values for the nape extension (for lower helmet mass), and two larger values for static spacing (for greater protection against back face deflection) are considered. Note, in this section, the original threat velocity of 364 m/s, based on the V_0 value of helmet A, and is used again. Thus, we will expect higher HIC values closer to the value of 254 calculated for helmet A.

Performing our analysis on each helmet gives the results shown in Fig. 11. The spacing modification has a large effect on the helmet performance and predicted injury. Recall that the BFD of the helmet is 25.4 mm and the dynamic spacing is the difference in the BFD attenuated by the obliquity of the impact and the static spacing. Thus, the result of increasing the mean static spacing directly produces higher dynamic spacing for all helmet impacts. Side opening and nape extension modifications had the predictable effect of slightly reducing overall helmet area and leading to a slightly higher number of fatal impacts as shown in Fig. 11(*b*). Since the spacing for those helmets was unchanged compared to the baseline, the mean dynamic spacing was relatively unchanged. Predicted AIS values remain relatively low and unchanged due to the modifications.

Table 3   Helmet A geometric modification summary

Helmet	Area (cm^2)	Mass (kg)	Geometry
A-S00-N37-H19 (baseline)	1077.3	1.16	
A-S00-N37-H22	1146.1	1.24	
A-S00-N37-H25	1219.1	1.32	
A-S00-N23-H19	988.7	1.07	
A-S00-N17-H19	939.7	1.02	
A-S20-N37-H19	1037.6	1.12	
A-S40-N37-H19	1022.2	1.11	

Comparing the performance of this set of helmets in terms of dynamic spacing versus HIC (Fig. 12) shows expected trends consistent with Fig. 11. Increasing the static spacing increases the mean dynamic spacing. This also increases the helmet area and mass to yield a lower HIC and an overall higher performance. Removing material from the helmet and reducing the mass has the opposite effect.

Study 3—Addition of Ceramic Applique. In the final study, the baseline helmet A is modified by adding a ceramic applique. With the addition of a ceramic applique, the protection, helmet mass, and inertia are increased significantly. The applique also allows for consideration of the more substantial 7.62 mm threat. The helmet geometry was divided into four zones (Table 4) to assess applique configuration trends on higher performance: lower front, upper front, upper back, and lower back. These individual zones were coded as X000, 0X00, 00X0, and 000X, respectively. Individual zones were designated by x equal to 0 for baseline aramid or x equal to 1 for the baseline aramid helmet plus the addition of the ceramic applique. Four one-zone applique helmet CAD models were created, i.e., 1000 (lower front), 0100 (upper front), 0010 (upper back), and 0001 (lower back) codes, to show how

individual zones influence helmet performance. Four additional two-zone applique models were created to demonstrate more practical combinations of zones, which would combine their influence on helmet performance. Using the nomenclature definitions, 1100 (front), 0011 (back), 0110 (upper), and 1001 (lower), two-zone applique configurations were incorporated into helmet CAD models and analyzed. Baseline aramid is designated by 0000 (baseline) and full aramid and applique by 1111 (complete). Applique areas and total helmet masses associated with these configurations are provided below each helmet configuration in Table 4.

Each of the ten helmet configurations was assessed using five 9 mm-to-7.62 mm threat sphere ratios between 100:0 and 0:100. The 9 mm threat velocity was again 364 m/s and the 7.62 mm threat velocity was 739 m/s. For brevity, only the results of 0:100, 50:50, and 100:0 are shown. The results of the one and two zone appliques are separated and compared to the 0000 (baseline) and 1111 (complete) configurations to better distinguish the performance trends and benefits.

As before, we first examine the histograms of the dynamic helmet spacing. The addition of a second threat type and material with different V_0 and BFD produces multiple peaks on the histograms; a distinct difference from the previous analyses. This behavior is best illustrated in Figs. 13(c) and 13(d) showing three
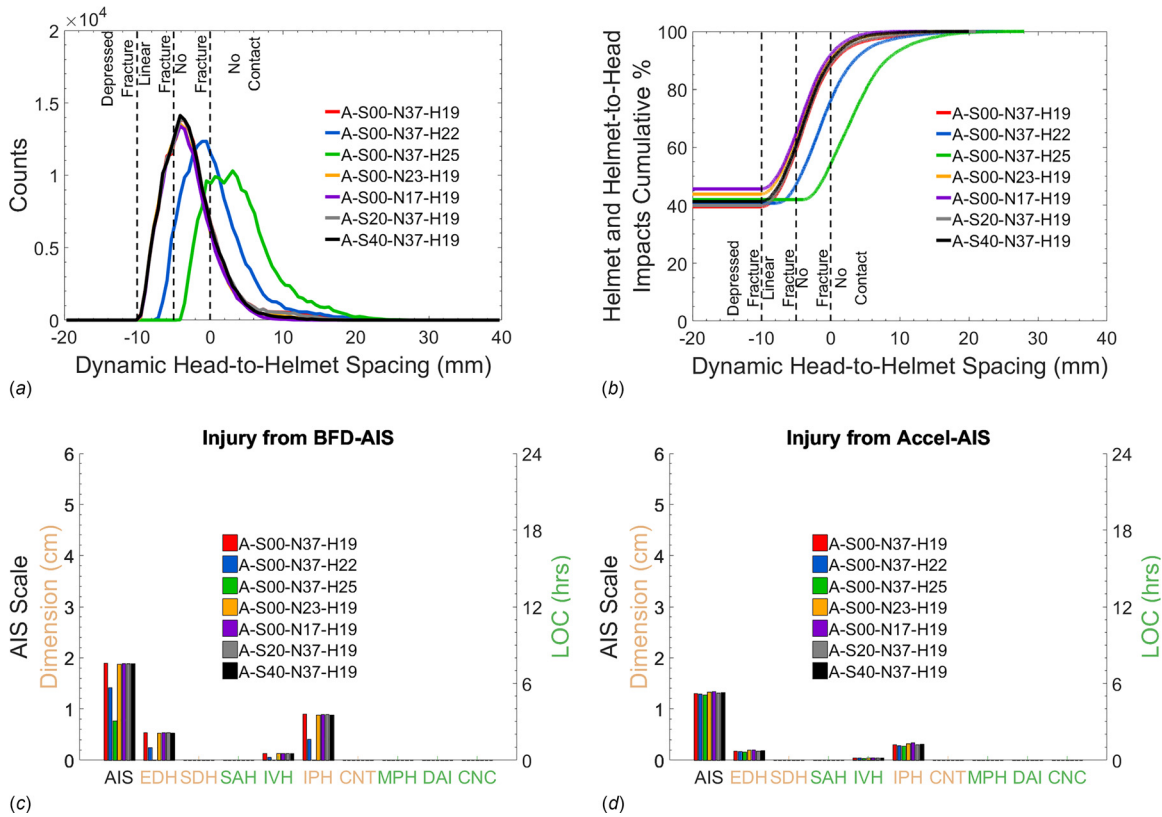
Fig. 11 Geometry modification parametric study performance for 9 mm strike velocity of 364 m/s: (*a*) helmet impact histograms, (*b*) all impact cumulative percentages (initial percentages are head impacts), (*c*) BFD-AIS, and (*d*) Accel-AIS and associated head injuries diagnosed by dimension or LOC duration

very distinct peaks. The leftmost peak (at −3 mm) is the 9 mm impacting the aramid, the middle peak (at 5 mm) is the 7.62 mm impacting the applique, and the rightmost peak (at 18 mm) is the 9 mm impacting the applique. Note that a fourth peak would be present if the 7.62 mm impacts did not fully penetrate the base aramid helmet shell.

It could be expected that the one zone applique with the largest area (0001 {lower back}) would have the highest performance by shifting the most number of impacts into the no-contact region. However, this behavior is not seen and the 0100 (upper front)

applique appears to perform the best followed by the 0010 (upper back) applique. The two zone applique shows much of the same behavior with regions covering the 1100 (front) and 0110 (upper) regions of the head having a higher performance but with lower or equivalent areas to the 0011 (back) and 1001 (lower) helmets. Applique size and location determine performance and both must be considered relative to the head and brain volume.
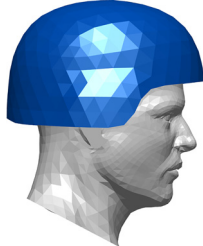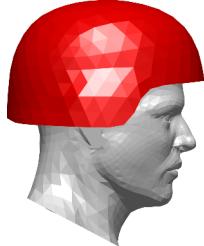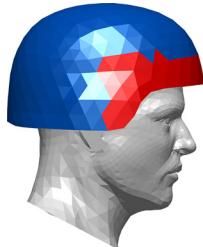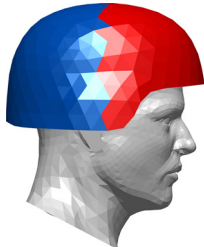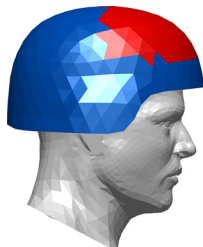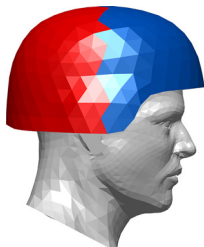
We now examine the cumulative impacts to the head–helmet system (Fig. 14). By implementing 7.62 mm threats into the analysis, complete penetrations through the helmet are now possible and a higher number of catastrophic impacts are seen. The difference between d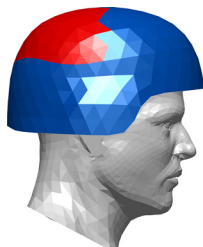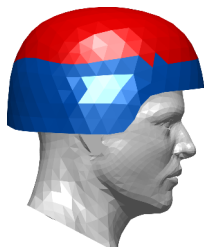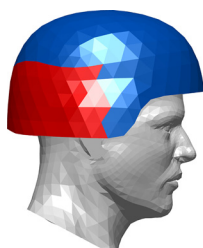irect catastrophic impacts and complete penetrating catastrophic impacts on helmet areas without applique coverage is highlighted by a second vertical offset after the head impacts region. The number of complete penetrating impacts shows the effect of applique area on performance. It is interesting to note the results of the 50:50 threat sphere percentage of penetrating impacts for the 0001 (lower back) applique compared to the 1100 (front) and 0110 (upper) appliques. While the area of the 0001 (lower back) configuration is lower than both of the 1100 (front) and 0110 (upper) configurations, the percentage of penetrating impacts is almost identical at approximately the same dynamic head-to-helmet spacing. This again highlights the need to consider both area and location in the applique design process to protect the brain from an anisotropic distribution of threats.

The dynamic spacing is approximately the same or higher than the previous cases, so we can see that the injury due to BFD calculations is approximately the same or lower than before. However, due to the high velocity of the 7.62 mm threat, the HIC values are significantly higher (Fig. 15(*a*)) and indicate a significant injury (Fig. 15(*b*)). An impact essentially at muzzle velocity from that 15 m range is generally considered to be very injurious or fatal. To represent a more realistic tactical situation in which the threat
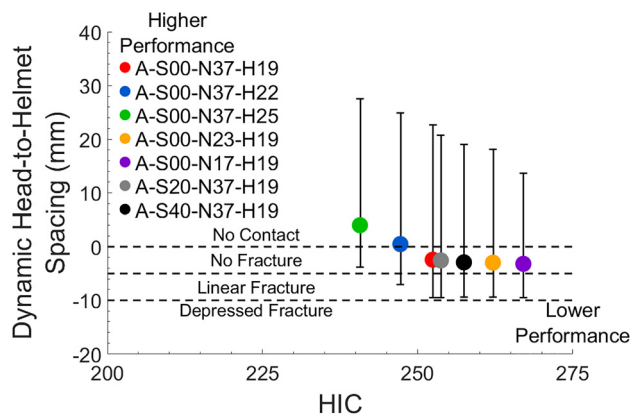
Fig. 12 Geometry modification parametric study analysis summary plot of dynamic spacing versus HIC value. Mean value and min–max represented by symbol and range for 9 mm strike velocity of 364 m/s.

Table 4 Baseline helmet, baseline augmented with full applique, four one-zone applique, and two-zone applique configurations


0 cm^2	0000 (Baseline)	1.16 kg	1077.3 cm^2	1111 (Complete)	2.53 kg
194.4 cm^2	1000 (Lower front)	1.41 kg	475.8 cm^2	1100 (Front)	1.77 kg
281.43 cm^2	0100 (Upper front)	1.52 kg	601.5 cm^2	0011 (Back)	1.93 kg
264.8 cm^2	0010 (Upper back)	1.50 kg	546.2 cm^2	0110 (Upper)	1.86 kg
336.7 cm^2	0001 (Lower back)	1.59 kg	531.1 cm^2	1001 (Lower)	1.84 kg

Note: The area of the applique and the total helmet mass are given below each helmet. Blue helmet areas are the baseline material and red areas are the baseline material augmented with a ceramic applique.

is fired from a longer distance, the threat velocity is reduced to 90, 80, and 70% V_0. This corresponds to stand-off distances of 70, 150, and 250 m. The reductions in predicted AIS for each of the velocity reductions are shown in Fig. 15(b).

A significant decrease in HIC (as much as 80%) and AIS (as much as 60%) values is predicted for the reduced velocities. Even the reduced values are still far greater than the AIS due to the fragment (i.e., 9 mm) impact. The HIC is reduced by an order of magnitude, while the AIS is reduced by at least half. Again, noting that the dynamic spacing values are similar or lower than those obtained by a 9 mm impact, we can determine if an injury occurred from the impact of a 7.62 mm threat. Such an injury would be due to motion of the head–helmet system, rather than deformation of the helmet and skull.
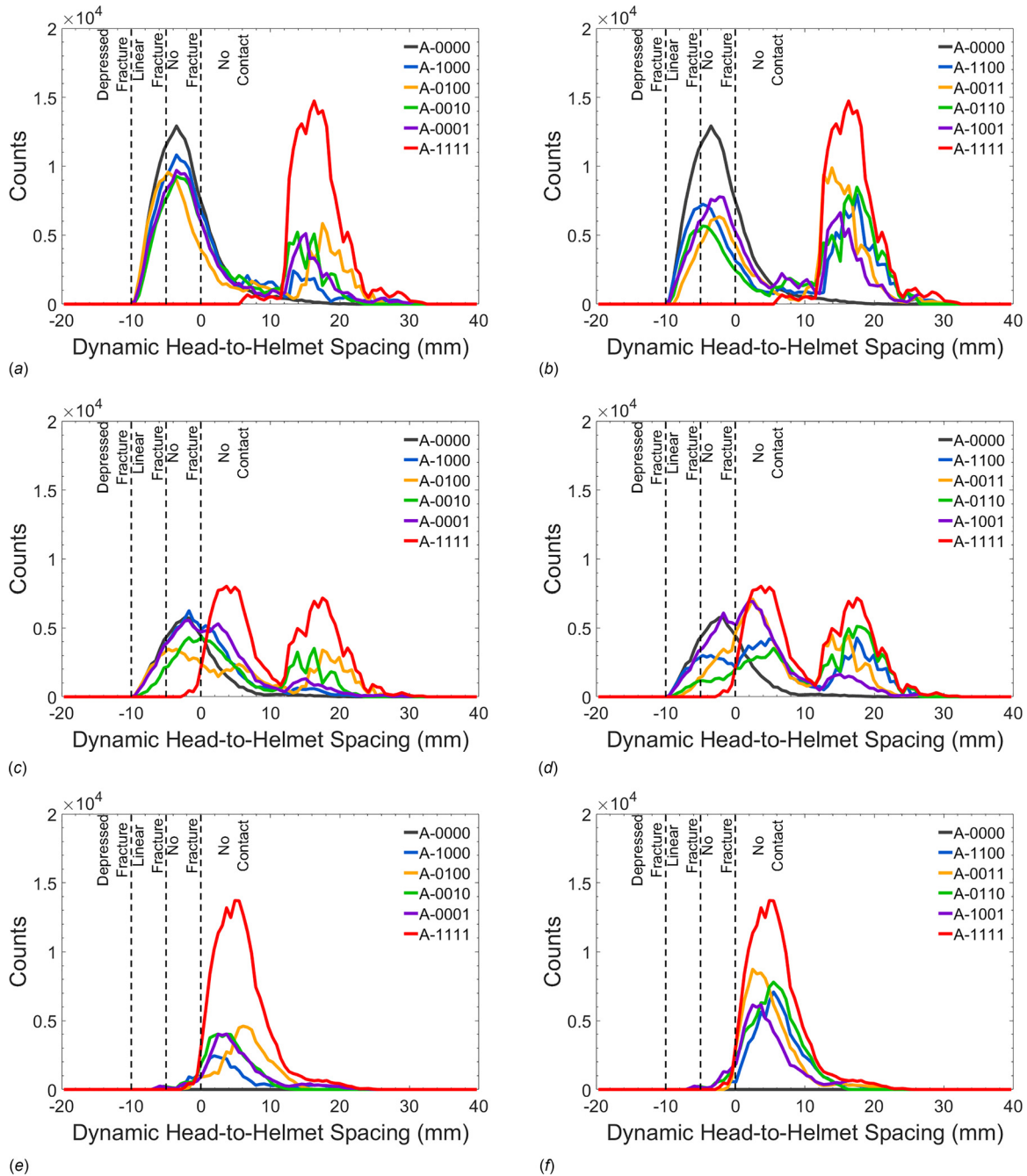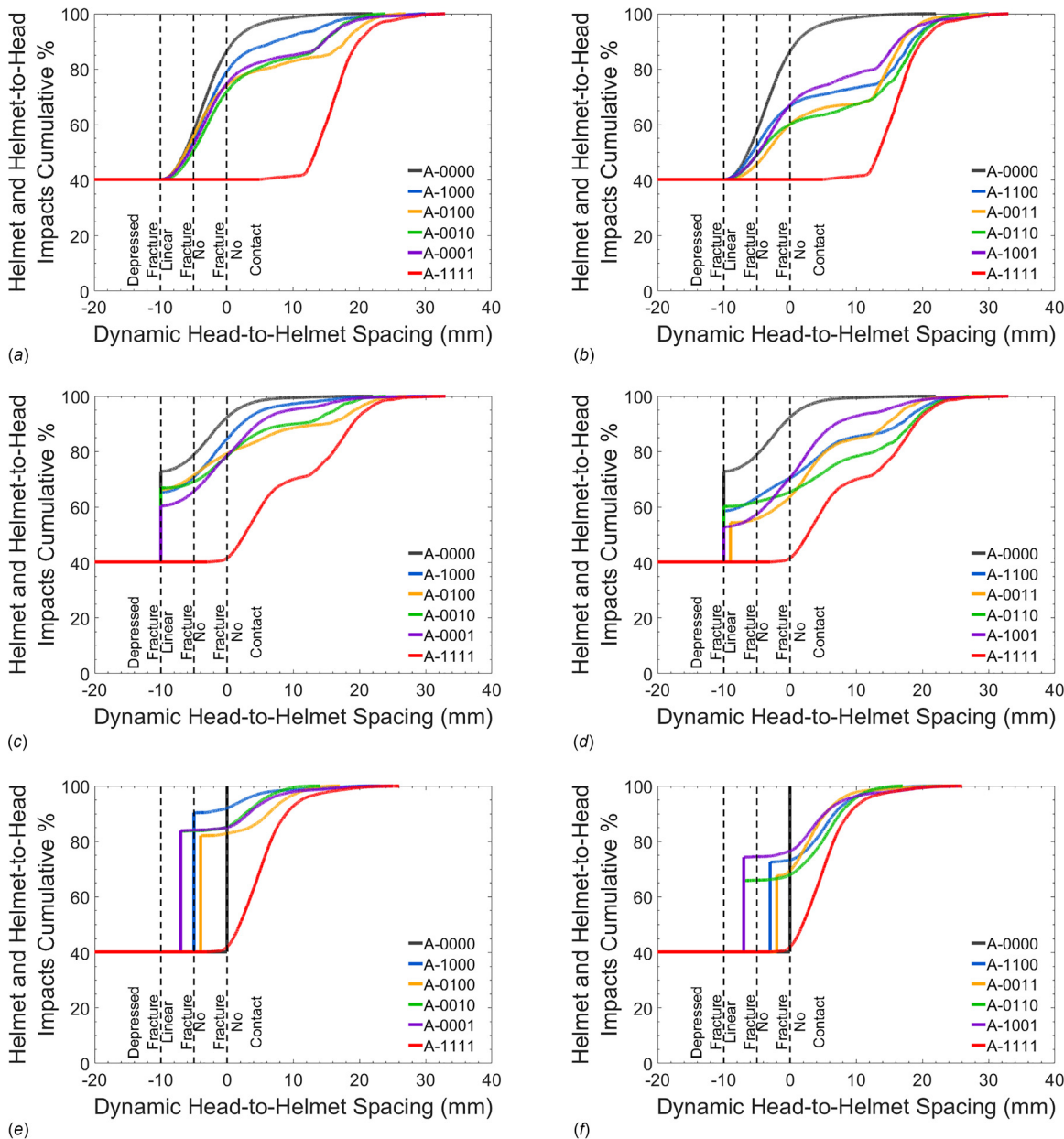
Fig. 13 Histograms of dynamic head-to-helmet spacing impacts for the baseline helmet, full coverage applique, one zone applique (left column plots (*a*), (*c*), and (*e*)) and two zone applique (right column plots (*b*), (*d*), and (*f*)) against threat sphere distributions of 0:100 (top row plots (*a*) and (*b*)), 50:50 (middle row plots (*c*) and (*d*)), and 100:0 (bottom row plots (*e*) and ((*f*) for 9 mm strike velocity of 364 m/s and 7.62 mm strike velocity of 739 m/s

Summary

A practical and modular CAD software application for helmet design has been developed and applied to generate comparative analyses of different combat helmet designs, parametric analyses of helmet geometry design parameters, and parametric analyses of ceramic applique configurations. The analyses have been used to assess the possibility of skull fracture based on BFD and nine head injuries (six internal focal injuries and three internal diffuse injuries) based on AIS values obtained from BFD and HIC values. The CAD software application incorporates a functionally representative set of points representing the brain volume. These 104 brain and spine points are paired with 3000 omni-directional ballistic threats at a distance. Basic ballistic experimental data, first order models, and head–helmet response dynamics are used to calculate the performance metrics. The program can analyze a single design, using the full set of ballistic threats, in a matter of minutes. This enables future extensive design analysis over a few hours using a common desktop computer.

The software has been used to generate a baseline performance for an aramid helmet designated helmet A using a relatively modest 9 mm threat with 344 m/s impact velocity to represent a fragment threat. The baseline helmet was then compared to four other helmets, helmets B–E, showing the effects of helmet geometry, head coverage, and material properties. Injury from back face deflection showed relatively minor injury in all cases, AIS < 2.5,

Fig. 14 Cumulative histograms of dynamic head-to-helmet spacing for the baseline helmet and full coverage applique compared to one zone applique (left column plots (*a*), (*c*), and (*e*)) and two zone applique (right column plots (*b*), (*d*), and (*f*)) against threat sphere distributions (fragment: small arms) of 0:100 (top row plots (*a*) and (*b*)), 50:50 (middle row plots c and (*d*), and 100:0 (bottom row plots (*e*) and (*f*) for 9 mm strike velocity of 364 m/s and 7.62 mm strike velocity of 739 m/s

but the injury predictions for each helmet were noticeably different showing the relative performance of one helmet compared to another. In all cases, a relatively minor and similar injury was predicted based on motion generated HIC values.

Next, six geometric modifications were made to the baseline helmet to examine their effect on performance against a 9 mm threat with a 364 m/s impact velocity. The results showed, by increasing the spacing and consequently the area of the helmet, a significant increase in helmet performance was obtained. The addition of the side opening and the removal of nape coverage had the opposite but slightly smaller effect and the HIC was increased due to the decrease in helmet mass, while fatal impacts increased due to the lower helmet area and associated head coverage. The dynamic spacing and injury prediction were not significantly affected by the changes to the helmet. This study of geometric parameters allows

designers to evaluate helmet coverage versus function tradeoffs to make more informed design choices.

In the final study, the baseline helmet was augmented with different configurations of a higher ballistic resistance ceramic applique. These helmet configurations were subjected to a threat sphere with both 9 mm threats at 364 m/s and 7.62 mm threats at 739 m/s representing fragments and small arms. The data were quantified and highlighted: the effects of helmet applique configurations on reducing complete penetrations by small arms, the challenges of protecting against high velocity small arms threats at short range, the role of fragment generated large BFD values in baseline BFD contact injuries, and the comparatively less severe injuries from fragment threats.

A number of additions and improvements are under consideration including additional metrics to rank threat trajectories in
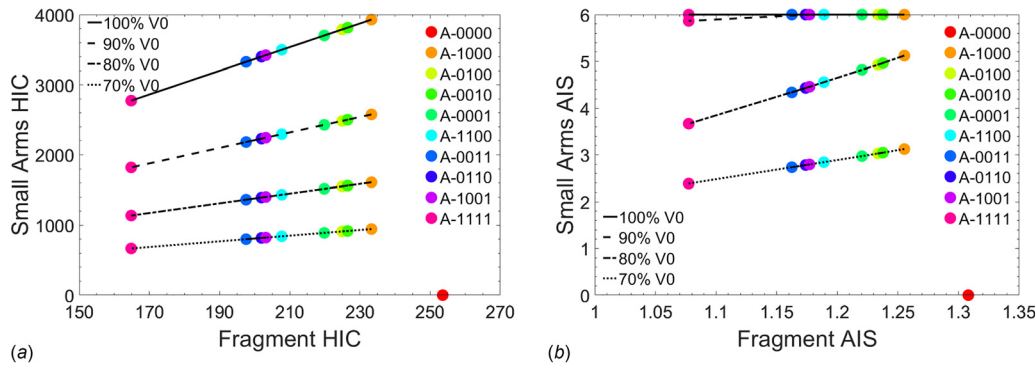
Fig. 15 Helmet applique configuration effects on helmet performance for ballistic resistance V_0 impact velocities and 0.9, 0.8, and 0.7 V_0 reduced impact velocities for the small arms threat: (*a*) small arms impact HIC versus fragment impact HIC and (*b*) small arms impact AIS versus fragment impact AIS (small arms baseline helmet sustains 100% catastrophic impacts, so no HIC or AIS can be calculated)

terms of risk to the brain, more descriptive metrics linking helmet impact and brain injury locations, and rotational acceleration injury criteria [25–27]. These types of additions will enhance the capabilities and provide additional capabilities for and insights into helmet design and optimization strategies.

Acknowledgment

References

[1] Li, X. G., Gao, X. L., and Kleiven, S., 2016, "Behind Helmet Blunt Trauma Induced by Ballistic Impact: A Computational Model," Int. J. Impact Eng., **91**, pp. 56–67.

[2] Salimi Jazi, M., Rezaei, A., Karami, G., Azarmi, F., and Ziejewski, M., 2014, "A Computational Study of Influence of Helmet Padding Materials on the Human Brain Under Ballistic Impacts," Comput. Methods Biomech. Biomed. Eng., **17**(12), pp. 1368–1382.

[3] Lee, H. P., and Gong, S. W., 2010, "Finite Element Analysis for the Evaluation of Protective Functions of Helmets Against Ballistic Impact," Comput. Methods Biomech. Biomed. Eng., **13**(5), pp. 537–550.

[4] Yang, J., and Dai, J., 2010, "Simulation-Based Assessment of Rear Effect to Ballistic Helmet Impact," Comput. Aided. Des. Appl., **7**(1), pp. 59–73.

[5] Tse, K. M., Tan, L. B., Yang, B., Tan, V. B. C., and Lee, H. P., 2016, "Effect of Helmet Liner Systems and Impact Directions on Severity of Head Injuries Sustained in Ballistic Impacts: A Finite Element (FE) Study," Med. Biol. Eng. Comput., **55**(4), pp. 641–662.

[6] Tan, L. B., Tse, K. M., Lee, H. P., Tan, V. B. C., and Lim, S. P., 2012, "Performance of an Advanced Combat Helmet With Different Interior Cushioning Systems in Ballistic Impact: Experiments and Finite Element Simulations," Int. J. Impact Eng., **50**, pp. 99–112.

[7] Aare, M., and Kleiven, S., 2007, "Evaluation of Head Response to Ballistic Helmet Impacts Using the Finite Element Method," Int. J. Impact Eng., **34**(3), pp. 596–608.

[8] Tham, C. Y., Tan, V. B. C., and Lee, H. P., 2008, "Ballistic Impact of a KEVLAR Helmet: Experiment and Simulations," Int. J. Impact Eng., **35**(5), pp. 304–318.

[9] Li, Y. Q., Li, X. G., and Gao, X.-L., 2015, "Modeling of Advanced Combat Helmet Under Ballistic Impact," ASME J. Appl. Mech., **82**(11), p. 111004.

[10] Walsh, S. M., Scott, B. R., Jones, T. L., Cho, K., and Wolbert, J., 2008, *A Materials Approach in the Development of Multi-Threat Warfighter Head Protection*, Army Research Lab, Aberdeen Proving Ground, MD.

[11] Hamouda, A. M. S., Sohaimi, R. M., Zaidi, A. M. A., and Abdullah, S., 2012, "Materials and Design Issues for Military Helmets," *Advances in Military Textiles and Personal Equipment* (Woodhead Publishing Series in Textiles), Elsevier, Amsterdam, The Netherlands, pp. 103–138.

[12] Kulkarni, S. G., Gao, X.-L., Horner, S. E., Zheng, J. Q., and David, N. V., 2013, "Ballistic Helmets—Their Design, Materials, and Performance Against Traumatic Brain Injury," Compos. Struct., **101**, pp. 313–331.

[13] Gordon, C. C., Blackwell, C. L., Bradtmiller, B., and Hotzman, J., 2013, "2010 Anthropometric Survey of U.S. Marine Corps Personnel: Methods and Summary," Army Natick Soldier Research, Development and Engineering Center, Natick, MA, Technical Report No. NATICK/TR-13/018.

[14] Brodmann, K., 1909, *Vergleichende Lokalisationslehre Der Grosshirnrinde in Ihren Prinzipien Dargestellt Auf Grund Des Zellenbaues*, J. A. Barth Verlag, Lepzig, Germany.

[15] Schmahmann, J. D., Doyon, J., McDonald, D., Holmes, C., Lavoie, K., Hurwitz, A., Kabani, N., Toga, A., Evans, A., and Petrides, M., 1999, "Three-Dimensional MRI Atlas of the Human Cerebellum in Proportional Stereotaxic Space," NeuroImage, **10**(3), pp. 233–260.

[16] Ford, M., Matic, P., and Leung, A., 2013, "Expanding Helmet Design Methodologies Through Brain Functional Area Representative Threat Models," ASME Paper No. IMECE2013-64959.

[17] Oishi, K., Faria, A., Jiang, H., Li, X., Akhter, K., Zhang, J., Hsu, J. T., Miller, M. I., van Zijl, P. C. M., Albert, M., Lyketsos, C. G., Woods, R., Toga, A. W., Pike, G. B., Rosa-Neto, P., Evans, A., Mazziotta, J., and Mori, S., 2009, "Atlas-Based Whole Brain White Matter Analysis Using Large Deformation Diffeomorphic Metric Mapping: Application to Normal Elderly and Alzheimer's Disease Participants," Neuroimage, **46**(2), pp. 486–499.

[18] Hisley, D. M., Gurganus, J. C., and Drysdale, A. W., 2011, "Experimental Methodology Using Digital Image Correlation to Assess Ballistic Helmet Blunt Trauma," ASME J. Appl. Mech., **78**(5), p. 051022.

[19] Tan, X. G., Saunders, R. N., and Matic, P., 2017, "Combat Helmet Pad Suspension Performance for Anthropomorphic Fit Designs and Injury Considerations," ASME Paper No. IMECE2017-70619.

[20] Blatt, A., and Bellis, E., 2004, "Tables of Potential Occult Injury Frequencies," Center for Transportation Injury Research, Buffalo, NY.

[21] Washington State Department of Health, CHS, 2011, "Washington State Hospital Data Dictionary—Version CVW4 (DOH 530-124)," Washington State Department of Health, CHS, Olympia, WA, pp. 123–128.

[22] Payne, A. R., and Patel, S., 2001, "Occupant Protection and Egress in Rail Systems," Mot. Ind. Res. Assoc.

[23] Matic, P., Moser, A. E., and Saunders, R. N., 2016, "A Combat Helmet Computer Aided Design Strategy Incorporating Ballistic Threat, Brain Functional Areas and Injury Considerations," Personal Armour Systems Symposium, Amsterdam, The Netherlands, Sept. 19–23.

[24] Matic, P., Moser, A. E., and Saunders, R. N., 2016, "Combat Helmet Design Incorporating Multiple Ballistic Threats, Brain Functional Areas and Injury Considerations," ASME Paper No. IMECE2016-67364.

[25] Takhounts, E. G., Craig, M. J., Moorhouse, K., McFadden, J., and Hasija, V., 2013, "Development of Brain Injury Criteria (BrIC)," Stapp Car Crash J., **57**, pp. 243–266.

[26] Rowson, S., and Duma, S. M., 2012, "The Virginia Tech Response," Ann. Biomed. Eng., **40**(12), pp. 2512–2518.

[27] Kimpara, H., and Iwamoto, M., 2012, "Mild Traumatic Brain Injury Predictors Based on Angular Accelerations During Impacts," Ann. Biomed. Eng., **40**(1), pp. 114–126.